Part 3: Synthesis Gas Production from CO_2-Containing Natural Gas by Combined Steam Reforming and Partial Oxidation in an AC Gliding Arc Discharge (submitted to *Plasma Chemistry and Plasma Processing*)

3.1 Introduction and Survey of Related Literature

In the recent years, research on the natural gas conversion to synthesis gas and fuels by using reforming processes has been extensively investigated [1-6]. These studies have been based on the reforming of pure CH_4 while natural gas contains not only CH_4 but also significant amount of ethane (C_2H_6), propane (C_3H_8) and carbon dioxide (CO_2). It is known that most natural gas, with a high concentration of carbon dioxide, has been found in Asia [7]. Hence, the reforming of natural gas composed of various components without a separation process is of great interest since it can result in a reduction of the high cost of the separation process and the net emission of CO_2.

Several techniques, such as steam reforming and partial oxidation, have been developed for methane reforming; however, they still possess some problems and constraints. The most extensively investigated method for hydrogen (H_2)/synthesis gas production from methane is steam reforming. Methane reforming with steam is a direct reaction between steam and methane to achieve a gaseous product with a higher H_2 content (Equation 1). Since steam methane reforming is a highly endothermic reaction, a huge amount of supplied energy is required. The reaction normally takes place over a nickel catalyst at very high temperatures of about 425-550 °C [8].

$$CH_4 + H_2O \rightarrow CO + 3H_2 \qquad \Delta H^0_{298} = +206\ kJ/mol \qquad (1)$$

The partial oxidation of methane is also an attractive alternative to converting

methane to H_2/synthesis gas. This reaction is an exothermic reaction (Equation 2); therefore, it can reduce the energy demand for the reforming reaction [9].

$$CH_4 + \frac{1}{2}O_2 \rightarrow CO + H_2 \qquad \Delta H^0_{298} = -36\ kJ/mol \qquad (2)$$

Apart from the aforementioned conventional processes, non-thermal plasma is a new efficient technique, which can be used for successfully converting natural gas into synthesis gas as well as other valuable products. Under ambient temperature and pressure, it provides highly active species (electrons, ions, and free radicals), which can initiate natural gas reforming reactions [10]. The gliding arc discharge originates from an auto-oscillating phenomenon that develops between at least two diverging electrodes submerged in a laminar or turbulent gas flow. The discharge starts as thermal plasma, and it quickly becomes non-thermal plasma during the space and time evolution. This powerful and energy-efficient transition discharge combines the benefits of equilibrium and non-equilibrium discharge characteristics in a single discharge pattern. So far, there are several research studies reporting the utilization of plasma discharge for hydrocarbon reforming [11-21]; however, to our knowledge, there have been no report on the combination of steam reforming and partial oxidation of CO_2-containing natural gas by using the gliding arc discharge system.

Therefore, the main objective of this work was to determine the roles of the gliding arc discharge plasma, in conjunction with the combined steam and partial oxidation, on the CO_2-containing natural gas reforming to produce synthesis gas. The experiments were systematically carried out to investigate the effects of several operating parameters, including the hydrocarbons (HCs)-to-O_2 feed molar ratio, applied voltage, input frequency, and electrode gap distance, on reactant conversions, product selectivities

and yields, and power consumptions in order to obtain optimum conditions for maximum synthesis gas production.

3.2 Procedure

3.2.1. Reactant Gases

The simulated natural gas used in this work consisted of CH_4, C_2H_6, C_3H_8, and CO_2, with a CH_4:C_2H_6:C_3H_8:CO_2 molar ratio of 70:5:5:20, and oxygen (O_2) were specially manufactured by Thai Industry Gas (Public) Co., Ltd.

3.2.2. AC Gliding Arc Discharge System

The schematic of a low-temperature gliding arc system used in this work is shown in Figure 3.1.

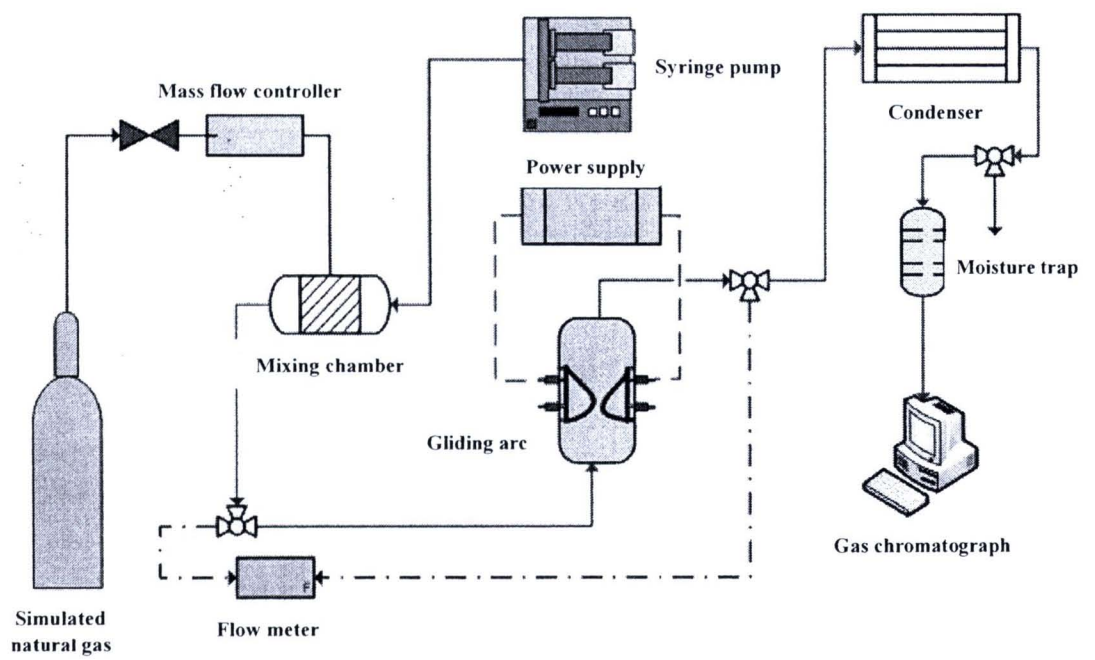

Figure 3.1 Schematic of gliding arc discharge system.

The detail of the gliding arc reactor configuration was described in our previous work [12]. A glass tube with 9 cm OD and 8.5 cm ID was used as the gliding arc reactor, which consisted of two diverging knife-shaped electrodes. The electrodes were made of stainless steel sheets with a 1.2 cm width. The gap distance between the pair of electrodes was fixed at 6 mm. The steam fed into the system was achieved by vaporizing water at a controlled temperature of 120 °C. A water flow rate was controlled by a syringe pump (Cole-Parmer). To prevent the water condensation in the feed line, the temperature of stainless tube from the syringe pump to a mixing chamber was maintained at 120 °C by using a heating tape. The flow rate of the simulated natural gas was controlled by a mass flow controller with a transducer (AALBORG). A 7-μm stainless steel filter was placed upstream of the mass flow controller in order to trap any solid particles in the reactant gas. The check valve was also placed downstream of the mass flow controller to prevent any backflow. The reactant gas and steam were well mixed in the mixing chamber controlled at 120 °C before being introduced upward into the reactor at atmospheric pressure. The compositions of the feed gas mixture and the outlet gas were quantitatively analyzed by an on-line gas chromatograph (HP, 5890) equipped with two separate columns, i.e. a Carboxen 1000 packed column and a PLOT Al_2O_3 "s" capillary column, which were adequate to detect all hydrocarbons, CO, CO_2, and H_2.

The power supply unit consisted of three steps. For the first step, the domestic AC input of 220 V and 50 Hz was converted to a DC output of 70 V by a DC power supply converter. For the second step, a 500 W power amplifier with a function generator was used to transform the DC into AC current with a sinusoidal waveform and different frequencies. For the third step, the outlet voltage was stepped up by using a high voltage transformer. The output voltage and frequency were controlled by the function generator.

The voltage and current at the low voltage side were measured instead of those at the high voltage side since the plasma generated is non-equilibrium in nature. The high side voltage and current were thereby calculated by multiplying and dividing by a factor of 130, respectively. A power analyzer was used to measure power, current, frequency, and voltage at the low voltage side of the power supply unit.

The feed gas mixture was first introduced into the gliding arc reactor without turning on the power supply unit for any studied conditions. After the compositions of outlet gas became invariant, the power supply unit was turned on. The flow rate of the outlet gas was also measured by using a bubble flow meter. The outlet gas was analyzed by the on-line GC every 30 min. After the plasma system reached steady state with invariant outlet gas concentrations, the outlet gas was taken for analysis at least a few times every hour. The average data were used to assess the process performance of the studied gliding arc discharge system.

3.2.3. Reaction Performance Calculation

The plasma system performance was evaluated from reactant conversions, product selectivities, H_2, CO, and C_2 yields, and power consumptions. The reactant conversion is defined as:

$$\% \text{ Reactant conversion} = \frac{(\text{Moles of reactant in} - \text{Moles of reactant out}) \times (100)}{\text{Moles of reactant in}} \quad (1)$$

The selectivity of any C-containing product is defined on the basis of the amount of C-containing reactants converted to any specified product, as stated in Equation 2. The percentage of coke formed can be calculated from the difference between the total reactant conversions and total C-containing products, as given in Equation 3. In the

instance of the H_2 product, its selectivity is calculated based on the amount of H-containing reactants converted, as stated in Equation 4:

$$\% \text{ Selectivity for any hydrocarbon product} = \frac{[P](C_P)(100)}{\Sigma[R](C_R)} \quad (2)$$

$$\% \text{ Selectivity for hydrogen} = \frac{[P](H_P)(100)}{\Sigma[R](H_R)} \quad (3)$$

where [P] = moles of product in the outlet gas stream

[R] = moles of each reactant in the feed stream to be converted

C_p = number of carbon atoms in a product molecule

C_R = number of carbon atom in each reactant molecule

H_p = number of hydrogen atoms in a product molecule

H_R = number of hydrogen atoms in each reactant molecule

The yields of various products are calculated using the following equations:

$$\% C_2 \text{ hydrocarbon yield} = \frac{[\Sigma(\% CH_4, \% C_2H_6, \% C_3H_8, \% CO_2 \text{ conversions})][\Sigma(\% C_2H_2, \% C_2H_4 \text{ selectivities})]}{(100)} \quad (4)$$

$$\% H_2 \text{ yield} = \frac{[\Sigma(\% CH_4, \% C_2H_6, \% C_3H_8 \text{ conversions})][\% H_2 \text{ selectivity}]}{(100)} \quad (5)$$

$$\% CO \text{ yield} = \frac{[\Sigma(\% CH_4, \% C_2H_6, \% C_3H_8, \% CO_2 \text{ conversions})][\% CO \text{ selectivity}]}{(100)} \quad (6)$$

The power consumption is calculated in a unit of Ws per C-containing reactant

molecule converted and Ws per hydrogen molecule produced using the following equation:

$$\text{Power consumption} = \frac{P \times 60}{N \times M} \tag{7}$$

where P = power (W)

N = Avogadro's number (6.02×10^{23} molecule g mole^{-1})

M = rate of converted carbon in the rate of produced hydrogen molecules (g mole min^{-1})

3.3 Results and Discussion

In order to obtain a better understanding of the chemical reactions in a plasma environment, the possibilities of all chemical pathways, which occurred by the collisions between electrons and all reactants introduced in to the feed to produce H_2 and various hydrocarbon species are hypothesized as the following reactions [8, 10]:

Electron-carbon dioxide collisions:

$$e^- + CO_2 \rightarrow CO + O^- \tag{9}$$

$$e^- + CO_2 \rightarrow CO + O + e^- \tag{10}$$

$$e^- + CO \rightarrow C + O + e^- \tag{11}$$

Electron-methane collisions:

$$e^- + CH_4 \rightarrow CH_3 + H + e^- \tag{12}$$

$$e^- + CH_3 \rightarrow CH_2 + H + e^- \tag{13}$$

$$e^- + CH_2 \rightarrow CH + H + e^- \tag{14}$$

$$e^- + CH \rightarrow C + H + e^- \quad (15)$$

$$H + H \rightarrow H_2 \quad (16)$$

Electron-ethane collisions:

$$e^- + C_2H_6 \rightarrow C_2H_5 + H + e^- \quad (17)$$

$$e^- + C_2H_5 \rightarrow C_2H_4 + H + e^- \quad (18)$$

$$e^- + C_2H_4 \rightarrow C_2H_3 + H + e^- \quad (19)$$

$$e^- + C_2H_3 \rightarrow C_2H_2 + H + e^- \quad (20)$$

$$e^- + C_2H_6 \rightarrow CH_3 + CH_3 + e^- \quad (21)$$

Electron-propane collisions:

$$e^- + C_3H_8 \rightarrow C_3H_7 + H + e^- \quad (22)$$

$$e^- + C_3H_7 \rightarrow C_3H_6 + H + e^- \quad (23)$$

$$e^- + C_3H_8 \rightarrow C_2H_5 + CH_3 + e^- \quad (24)$$

Electron-water collisions:

$$e^- + H_2O \rightarrow O^- + H_2 \quad (25)$$

$$e^- + H_2O \rightarrow OH^- + H \quad (26)$$

Under the presence of oxygen, several chemical reactions can be initiated in the plasma environment as follows:

Dissociative attachment:

$$e^- + O_2 \rightarrow 2O + e^- \rightarrow O^- + O \quad (27)$$

Attachment:

$$e^- + O_2 \rightarrow O_2^- \quad (28)$$

Dissociation:

$$e^- + O_2 \rightarrow 2O + e^- \quad (29)$$

Oxidative dehydrogenation reactions:

$$CH_4 + O\ (O^-, O_2^-) \rightarrow CH_3 + OH\ (OH^-, HO_2^-) \quad (30)$$

$$C_2H_6 + O\ (O^-, O_2^-) \rightarrow C_2H_5 + OH\ (OH^-, HO_2^-) \quad (31)$$

$$C_2H_5 + O\ (O^-, O_2^-) \rightarrow C_2H_4 + OH\ (OH^-, HO_2^-) \quad (32)$$

$$C_2H_4 + O\ (O^-, O_2^-) \rightarrow C_2H_3 + OH\ (OH^-, HO_2^-) \quad (33)$$

$$C_2H_3 + O\ (O^-, O_2^-) \rightarrow C_2H_2 + OH\ (OH^-, HO_2^-) \quad (34)$$

$$C_3H_8 + O\ (O^-, O_2^-) \rightarrow C_3H_7 + OH\ (OH^-, HO_2^-) \quad (35)$$

$$C_3H_7 + O\ (O^-, O_2^-) \rightarrow C_3H_6 + OH\ (OH^-, HO_2^-) \quad (36)$$

$$CH_4 + OH\ (O^-, O_2^-) \rightarrow CH_3 + H_2O\ (OH^-, HO_2^-) \quad (37)$$

$$C_2H_6 + OH\ (O^-, O_2^-) \rightarrow C_2H_5 + H_2O\ (OH^-, HO_2^-) \quad (38)$$

$$C_2H_5 + OH\ (O^-, O_2^-) \rightarrow C_2H_4 + H_2O\ (OH^-, HO_2^-) \quad (39)$$

$$C_2H_4 + OH\ (O^-, O_2^-) \rightarrow C_2H_3 + H_2O\ (OH^-, HO_2^-) \quad (40)$$

$$C_2H_3 + OH\ (O^-, O_2^-) \rightarrow C_2H_2 + H_2O\ (OH^-, HO_2^-) \quad (41)$$

$$C_3H_8 + OH\ (O^-, O_2^-) \rightarrow C_3H_7 + H_2O\ (OH^-, HO_2^-) \quad (42)$$

$$C_3H_7 + OH\ (O^-, O_2^-) \rightarrow C_3H_6 + H_2O\ (OH^-, HO_2^-) \quad (43)$$

All the active species formed from either electron collisions and oxidative reactions can further react to form various products as follows:

Coupling reactions of active species:

Ethylene (C_2H_4) formation;

$$CH_2 + CH_2 \rightarrow C_2H_4 \quad (44)$$

$$CH_3 + CH_3 \rightarrow C_2H_4 + H_2 \quad (45)$$

$$C_2H_5 + H \rightarrow C_2H_4 + H_2 \quad (46)$$

$$C_3H_7 + H \rightarrow C_2H_4 + CH_4 \quad (47)$$

Acetylene(C_2H_2) formation;

$$CH + CH \rightarrow C_2H_2 \quad (48)$$

$$CH_2 + CH_2 \rightarrow C_2H_2 + H_2 \quad (49)$$

$$CH_3 + CH \rightarrow C_2H_2 + H_2 \quad (50)$$

$$C_2H_5 + H \rightarrow C_2H_2 + H_2 + H_2 \quad (51)$$

$$C_3H_7 + H \rightarrow C_2H_2 + CH_4 + H_2 \quad (52)$$

Butane (C_4H_{10}) formation;

$$C_2H_5 + C_2H_5 \rightarrow C_4H_{10} \quad (53)$$

$$C_3H_7 + CH_3 \rightarrow C_4H_{10} \quad (54)$$

Carbon monoxide (CO) formation:

$$CH_3 + O \rightarrow HCHO + H \quad (55)$$

$$HCHO + O \rightarrow OH + CHO \quad (56)$$

$$CHO + O \rightarrow OH + CO \quad (57)$$

$$CHO + OH \rightarrow CO + H_2O \quad (58)$$

$$CHO + H \rightarrow H_2 + CO \quad (59)$$

3.3.1. Effect of the Hydrocarbons (HCs)-to-O_2 Feed Molar Ratio

Typically, the HCs-to-O_2 feed molar ratio in the natural gas feed mixture has a considerable impact on the plasma characteristics (i.e. breakdown voltage, electrical conductivity, and physical appearance) and the plasma stability, depending on the properties of each gas component. In this work, the experiments were initially performed by varying the O_2 content in the feed to obtain various HCs-to-O_2 feed molar ratios of 2/1, 3/1, 4/1, 6/1, and 9/1, while the other operating parameters were controlled at the base conditions (a steam content of 10 mol%, a total feed flow rate of 100 cm^3/min, an applied voltage of 13.5 kV, an input frequency of 300 Hz, and an electrode gap distance of 6 mm)

[23]. In this plasma system, a HCs-to-O_2 feed molar ratio lower than 2/1 was not investigated since it is close to the explosion zone.

Figure 3.2 shows the process performance of the studied gliding arc system as a function of the HCs-to-O_2 feed molar ratio. A decrease in the HCs-to-O_2 molar ratio (a lower HCs-to-O_2 feed molar ratio means a higher O_2 content) significantly enhanced both the conversions of all reactants (except CO_2) and the yields of H_2, CO, and C_2. The results can be explained by the fact that, when O_2 presents in the plasma system, it plays an important role in providing O_2 active species from the dissociative attachment reactions, as shown in Equations 27-29. These O_2 active species can further activate all reactants by oxidative dehydrogenation reactions (Equations 30-43), leading to an increase in the conversions of CH_4, C_2H_6, and C_3H_8, as well as the H_2, CO, and C_2 yields. An increase in O_2 content in the feed (decreasing HCs/O_2 feed molar ratio) results in the enhancement of a complete combustion reaction, leading to a decrease in CO_2 conversion.

As shown in Figure 3.2b, the CH_4, C_2H_6, and C_3H_8 concentrations in the outlet gas decrease significantly with decreasing HCs-to-O_2 feed molar ratios whereas the concentration of CO increases drastically with a slight increase in H_2 concentration. Interestingly, the CO_2 conversion decreased with the decreasing HCs-to-O_2 feed molar ratio. As mentioned before, when decreasing the HCs-to-O_2 feed molar ratio, the increase in oxygen provides a higher possibility for the oxidation of hydrocarbons to CO_2. Therefore, negative aspect of the CO_2 conversion at the lowest HCs-to-O_2 feed molar ratio of 2/1 suggests that the system provides a higher formation rate of CO_2 by the complete hydrocarbon oxidation than the CO_2 reduction rate by the reforming reactions [10]. In comparisons between the two cases of without and with O_2 addition in the feed,

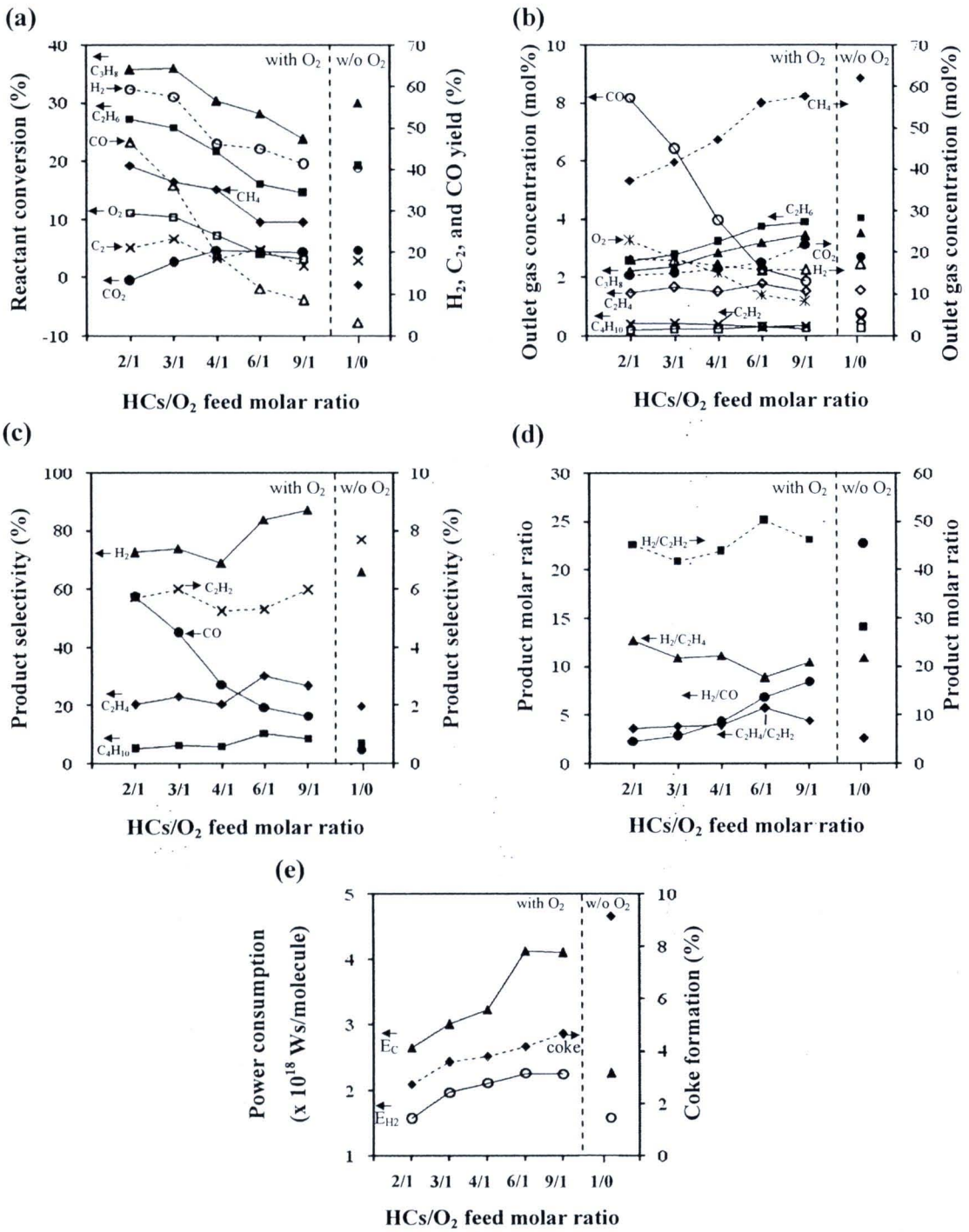

Figure 3.2 Effects of HCs-to-O_2 feed molar ratio on (a) reactant conversions and product yields, (b) concentrations of outlet gas, (c) product selectivities, (d) product

molar ratios, and (e) power consumptions and coke formation under studied conditions: steam content, 10 mol%; total feed flow rate, 100 cm^3/min; applied voltage, 13.5 kV; input frequency, 300 Hz; and electrode gap distance, 6 mm (E_c: power per reactant molecule converted; E_{H2}: power per H_2 molecule produced).

the O_2 addition in the feed with any HCs-to-O_2 feed molar ratio lower than 4/1 (high O_2 content range) potentially contributes to the positive effect of the enhancement of the reactant conversions, with the exception of the CO_2 conversion, and the H_2, CO, and C_2 yields, as well as the H_2 and CO selectivities.

The effect of the HCs-to-O_2 feed molar ratio on product selectivities is shown in Figure 3.2c. The selectivities for C_2H_4, C_4H_{10}, and H_2 tended to decrease with the decreasing HCs-to-O_2 feed molar ratio, whereas the CO selectivity increased drastically. As mentioned earlier, the higher the number of oxygen active species, the higher the opportunity for oxidative dehydrogenation reactions, consequently producing several intermediated species and water. Some of intermediate species (i.e. C_2H_5 and C_2H_3) can be further reacted to form C_2H_4 and C_2H_2 either by electron collisions (Equations 18, 20) and/or by oxidative dehydrogenation reactions (Equations 32, 34). In addition, the radicals of hydrocarbons and hydrogen derived from the earlier reactions may possibly react further to combine with one another via coupling reactions to form H_2, C_2H_2, C_2H_4, and C_4H_{10}, as shown in Equations 44-54. Hence, with the decreasing tendencies of the H_2, C_2H_2, C_2H_4, and C_4H_{10} selectivities with decreasing HCs-to-O_2 feed molar ratios infer that the opportunity for coupling reactions to form higher hydrocarbon molecules is less favorable at a lower HCs-to-O_2 feed molar ratio. The increase in the CO selectivity with decreasing HCs-to-O_2 feed molar ratio can be explained by the fact that the higher O and

OH active species may possibly provide a higher possibility of the partial oxidative pathways forming CO as an end product (Equations 55-59).

Figure 3.2d shows the effects of the HCs-to-O_2 feed molar ratio on various product molar ratios. The molar ratios of H_2/CO, H_2/C_2H_2, and C_2H_4/C_2H_2 tended to decrease with decreasing HCs-to-O_2 feed molar ratios, while the H_2/C_2H_4 molar ratio showed the opposite trend. These results correspond well to the decreases in the H_2, C_2H_4, and C_4H_{10} selectivities and the increase in the CO selectivity with the decreasing HCs-to-O_2 feed molar ratio. The increase in the H_2/C_2H_4 molar ratio with the increasing O_2 ratio in the system (decreasing the HCs-to-O_2 feed molar ratio) implies that the oxidative dehydrogenation reactions of hydrocarbons to form smaller hydrocarbon molecules have higher possibilities to simultaneously occur, as compared to the coupling reactions of active species to form large hydrocarbon molecules.

The effects of the HCs-to-O_2 feed molar ratio on power consumptions and coke formation are illustrated in Figure 3.2e. The power consumptions of both per reactant molecule converted and per H_2 molecule produced declined drastically with the decreasing HCs-to-O_2 feed molar ratio. The drop in both power consumptions can be explained by the increases in the CH_4, C_2H_6, and C_3H_8 conversions and H_2 yield (Figure 3.2a). Moreover, a decreasing tendency of coke deposition on the electrode surfaces and inner reactor glass wall could be observed at lower HCs-to-O_2 feed molar ratios (with higher O_2 contents). From the overall results, the optimum HCs-to-O_2 feed molar ratio of 2/1, which reasonably provided both higher H_2 yield and selectivity with extremely low power consumptions, was selected for further investigation. It is interesting to point out that the addition of oxygen cannot reduce the power consumption but it can significantly decrease coke formation.

3.3.2. Effect of Applied Voltage

In general, the applied voltage plays a significant role on plasma behaviors and subsequent plasma chemical reaction performance. For the investigated plasma system, the highest operating applied voltage of 20.5 kV was limited by the plasma instability and thereby the extinction of gliding arc discharges due to a very large amount of rapid coke deposited on the electrode surface. The lowest applied voltage (break-down voltage) to generate steady plasma was found at 13.5 kV. Hence, the experiments were carried out to investigate the effect of applied voltage in the range of 13.5-20.5 kV, while the other operating parameters were kept constant at a steam content of 10 mol%, a HCs-to-O_2 feed molar ratio of 2/1, a total feed flow rate of 100 cm^3/min, an input frequency of 300 Hz, and an electrode gap distance of 6 mm. The effects of applied voltage on the reactant conversions and product yields are demonstrated in Figure 3.3a. The conversions of CH_4, C_2H_6, C_3H_8, and O_2, as well as the H_2 and CO yields, steadily increased with increasing applied voltage. However, the CO_2 conversion remained almost unchanged in the studied range of applied voltage. These reactant conversion results were consistent with the decreases in the CH_4, C_2H_6, C_3H_8, and O_2 concentrations in the outlet gas, as well as the increases in H_2 and CO concentrations (Figure 3.3b). Fundamentally, an increase in the applied voltage for a plasma system directly corresponds to a stronger electric field strength across the electrodes, resulting in higher electron density or higher input energy (current) to the system [10], as indicated in Figure 3.3c. Increasing applied voltage leads to an increased opportunity for the occurrence of elementary chemical reactions by electron collision, by resulting in increases in all the conversions of CH_4, C_2H_6, C_3H_8, and O_2, as well as the H_2 and CO yields. The unchanged CO_2 conversion and CO_2

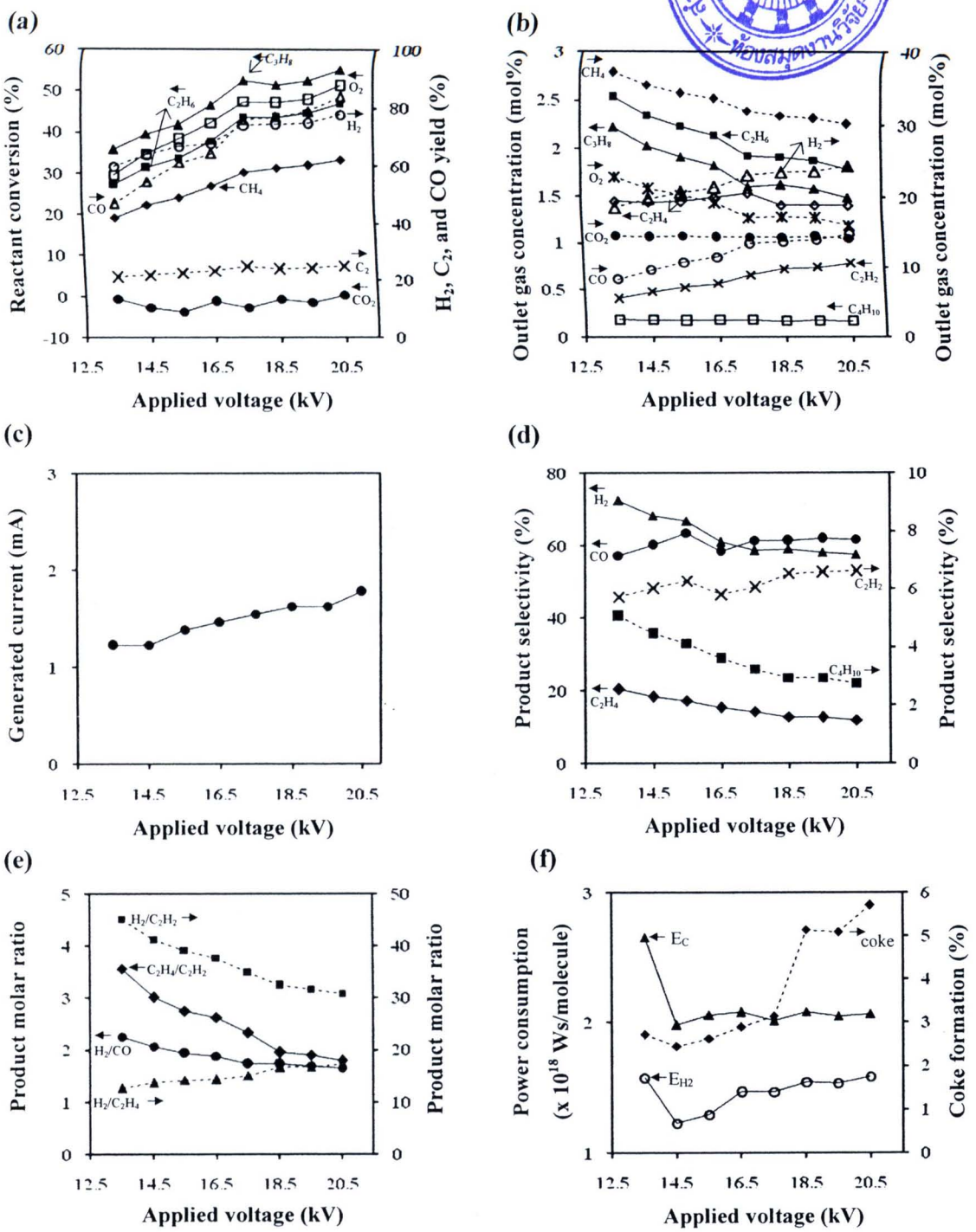

Figure 3.3 Effects of applied voltage on (a) reactant conversions and product yields, (b) concentrations of outlet gas, (c) generated current, (d) product selectivities, (e) product molar ratios, and (f) power consumptions and coke formation under studied

conditions: steam content, 10 mol%; HCs/O_2 feed molar ratio, 2/1; total feed flow rate, 100 cm^3/min; input frequency, 300 Hz; and electrode gap distance, 6 mm (E_c: power per reactant molecule converted; E_{H2}: power per H_2 molecule produced).

concentration in the product gas suggest that the rate of CO_2 reforming by plasma should be equal to the rate of CO_2 formation by the complete combustion reaction. In the applied voltage range of 18.5-20.5 kV, the slight increases in the CH_4, C_2H_6, C_3H_8, and O_2 conversions and the H_2 and CO yields can be credited to the increase in coke formation (as shown later), which was observed to be an obstacle to maintaining steady plasma behavior. Besides, it was found that increasing applied voltage had an insignificant impact on the C_2 yield, possibly, suggesting that the C_2 yield was independent of an applied voltage in the investigated range.

Figure 3.3d presents the effects of applied voltage on the product selectivities. The H_2, C_2H_4, and C_4H_{10} selectivities decreased with increasing applied voltage, whereas the C_2H_2 and CO selectivities tended to increase. These results imply that at a higher applied voltage, the carbon dioxide dissociation by electron collision (Equations 9 and 10) and oxidative dehydrogenation reactions of the hydrocarbons (Equations 30-43) occur more often than the coupling reactions of active species (Equations 44-54). According to the plasma behavior observed, a higher applied voltage can induce greater electron density and subsequently a higher number of active species, which can increased opportunity for both carbon dioxide dissociation and oxidative dehydrogenation reactions.

The effect of applied voltage on the product molar ratios is illustrated in Figure 3.3e. The molar ratios of H_2/CO, H_2/C_2H_2, and C_2H_4/C_2H_2 substantially decreased with

increasing applied voltage, while the H_2/C_2H_4 molar ratio showed the opposite trend. These results agree well with the decreased H_2, C_2H_4, and C_4H_{10} selectivities and the increased C_2H_2 and CO selectivities. The apparent decreases in the H_2/C_2H_2, H_2/CO, and C_2H_4/C_2H_2 molar ratios, and the opposite trend of the H_2/C_2H_4 molar ratio with increasing applied voltage, again confirm that the carbon dioxide dissociation by electron collision and oxidative dehydrogenation reactions are much more likely to occur than the coupling reactions of active species with increasing applied voltage.

Figure 3.3f shows the effects of applied voltage on power consumptions and coke formation. The power consumptions of both per reactant molecule converted and per H_2 molecule produced, decreased with increasing applied voltage (from 13.5 to 14.5 kV); however, with further increasing applied voltage to 20.5 kV, the power consumption per reactant molecule converted tended to be fairly constant, while the power consumption per H_2 molecule produced tended to only slightly increase. The initial decreases in both amounts of power consumptions can be explained by the increases in the CH_4, C_2H_6, and C_3H_8 conversions and the H_2 yield with increasing applied voltage. When considering the applied voltage range of 14.5-20.5 kV, the results reveal that the power consumption per H_2 molecule produced increased steadily with increasing applied voltage. The increase in H_2 yield with increasing applied voltage should indeed have led to lower power consumption per H_2 molecule produced. However, the opposite trend was experimentally observed, possibly because of the increase in coke formation. Generally, the formation of coke along the knife-shaped electrodes at high applied voltages not only decreases the efficiency of chemical reactions (i.e. decreasing reactant conversions and product yields) but also directly affects the gliding arc discharge stability. Particularly, an increase in a certain amount of coke can increase the conductivity of the system, leading to a decrease

in the uniformity of the plasma pattern. This phenomena resulted in a lowered probability of electron collision with reactant molecules to produce active gaseous species. From the results, a minimum of power consumptions were found at the applied voltage of 14.5 kV, while all ratios of hydrogen-to-other products were mostly high; therefore, the applied voltage of 14.5 kV was selected for further investigation.

3.3.3 Effect of Input Frequency

The input frequency parameter was next investigated by varying the range from 290-500 Hz, while the other operating parameters were controlled at a steam content of 10 mol%, a HCs/O_2 feed molar ratio of 2/1, a total feed flow rate of 100 cm^3/min, an applied voltage of 14.5 kV, and an electrode gap distance of 6 mm. It should be noted that the studied gliding arc system could not be operated lower than the lowest operating input frequency of 290 Hz. This is because a large amount of coke formation occurred on the surface of the electrodes as well as the extremely high current. For the input frequency greater than 500 Hz, the plasma system could not be operated because of the non-uniform plasma with a extremely small number of arcs produced. Figure 3.4 illustrates the effects of input frequency on the reactant conversions, product yields, concentrations of outlet gas, and power consumptions. The conversions of CH_4, C_2H_6, C_3H_8, and O_2, as well as the H_2, CO, and C_2 yields, tended to decrease with increasing input frequency (Figure 3.4a). These results correspond well to the increases in CH_4, C_2H_6, C_3H_8, and O_2 concentrations, as well as the decreases in H_2 and CO concentrations in the outlet gas (Figure 3.4b). In general, for any given applied voltage and electrode gap distance, the

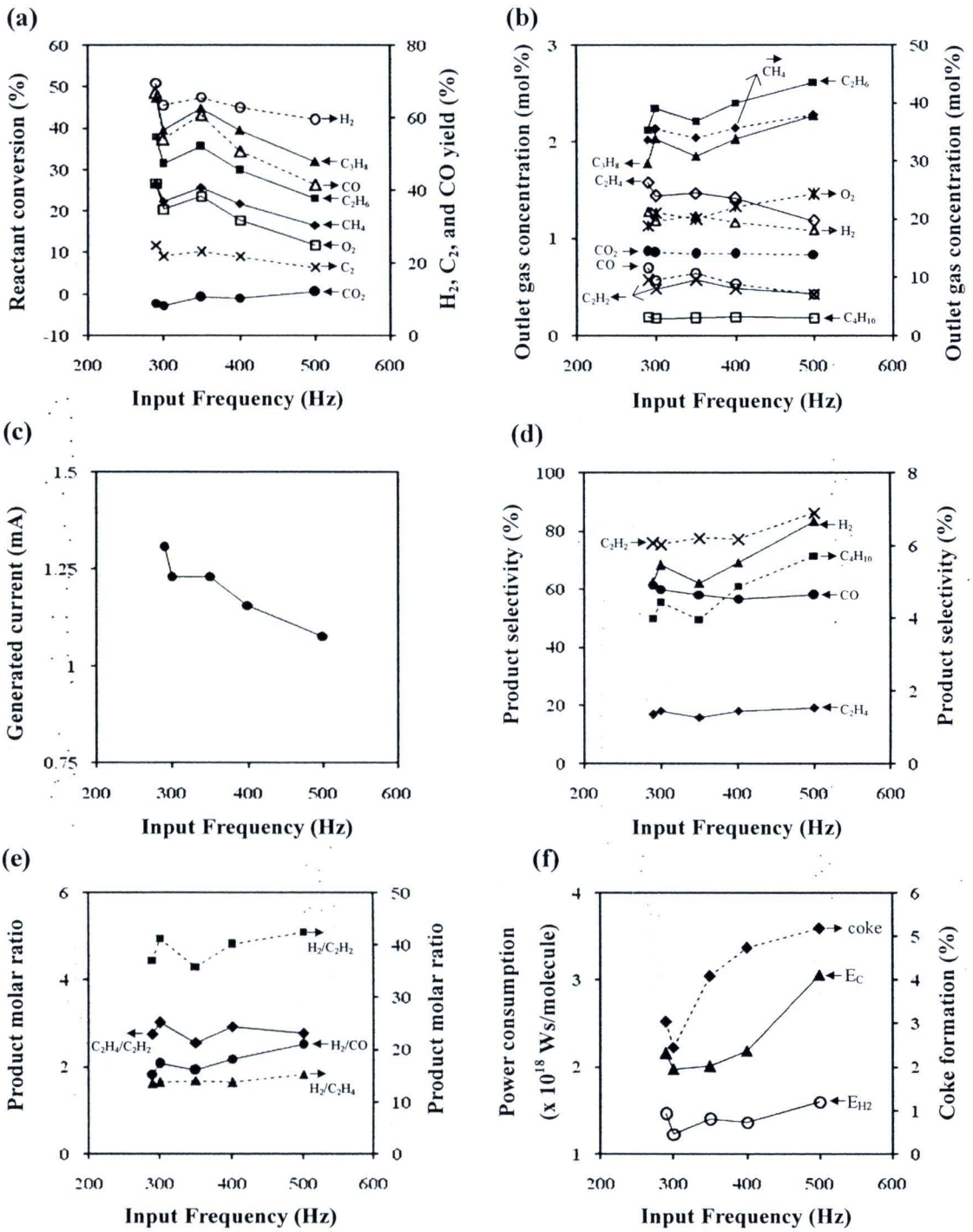

Figure 3.4 Effects of input frequency on (a) reactant conversions and product yields, (b) concentrations of outlet gas, (c) generated current, (d) product selectivities, (e) product molar ratios, and (f) power consumptions and coke

formation under studied conditions: steam content, 10 mol%; HCs/O_2 feed molar ratio, 2/1; total feed flow rate, 100 cm^3/min; applied voltage, 14.5kV; and electrode gap distance, 6 mm (E_c: power per reactant molecule converted; E_{H2}: power per H_2 molecule produced).

electric current required to sustain a discharge is reduced with increasing input frequency. Consequently, a lower current can be observed at a higher input frequency, as shown in Figure 3.4c. In accordance with the basic concept of the frequency effect as stated, the space charge (electrons and ions) characteristics of the alternating current discharge is the influential factor of frequency in changing the behaviors of arc discharge and reaction performance [8, 10, 24-25]. Therefore, increasing input frequency adversely causes a reduction in the number of electrons generated for initiating the chemically active species via the elementary plasma reactions by electron impact, resulting in lower reactant conversions and product yields.

The effect of input frequency on the product selectivities is shown in Figure 3.4d. The H_2, C_2H_2, and C_4H_{10} selectivities tended to increase with increasing input frequency from 290 to 500 Hz, whereas the C_2H_4 and CO selectivities tended to remain almost unchanged, implying that the C_2H_4 and CO selectivities were independent of input frequency. The present results do not agree with those in our previous work [10], in which the decreases in both H_2 and C_2H_2 selectivities were observed with increasing input frequency from 250-500 Hz. The difference in the experimental results could possibly be explained by the fact that the previous work used only simulated natural gas as a reactant feed, whereas the present work was conducted by adding both steam and oxygen to the simulated natural gas. Hence, the results imply that the presence of steam

and oxygen plays an important role in enhancing the electron-water collisions (Equations 25 and 26), as well as the dissociation reactions of oxygen (Equations 27-29), leading to increased oxidative dehydrogenation reactions (Equations 30-43) and coupling reactions of active species (Equations 44-54) to produce more H_2 and C_2H_2. As shown in Figure 4d, the increase in C_4H_{10} selectivity infers that the promotion of coupling reactions to form C_4H_{10} (Equations 53 and 54) can be achieved by increasing input frequency.

Figure 3.4e shows the effect of input frequency on the product molar ratios. The molar ratios of H_2/CO and H_2/C_2H_2 tended to increase with increasing input frequency. The increase in the H_2/CO molar ratio can be possibly described by the increase in the H_2 selectivity, while the CO selectivity remained almost unchanged with increasing input frequency. Interestingly, the simultaneous increases in the H_2/C_2H_2 molar ratio and the H_2 and C_2H_2 selectivities imply that the increase in the H_2 production rate is higher than that of the C_2H_2 production rate where the input frequency is increased. As a result, the number of electrons generated in the plasma system decreases with increasing input frequency, resulting in decreasing possibilities of secondary dehydrogenation reactions of hydrocarbon species (Equations 30-34 and 37-41) to produce C_2H_2. On the contrary, the H_2 selectivity increase with increasing input frequency is possibly due to the presence of steam, which provides a higher possibility of collision, between the electrons and water molecules (Equations 25-26). In addition, the C_2H_4/C_2H_2 molar ratio decreased slightly with increasing input frequency, whereas the H_2/C_2H_2 molar ratio remained almost unchanged. These results agree well with the increase in C_2H_2 selectivity and the invariant of C_2H_4 selectivity.

The effects of input frequency on power consumptions and coke formation are depicted in Figure 3.4f. The power consumptions of both per reactant molecule converted

and per H_2 molecule produced initially decreased with increasing input frequency from 290 to 300 Hz and then substantially increased with further increasing input frequency from 300 to 500 Hz. The initial decrease in both power consumptions was observed probably due to the decrease in current required to sustain the discharge (Figure 3.4c); whereas the further increase in input frequency from 300 to 500 Hz increased both power consumptions, probably resulting from the decreases in all reactant conversions and H_2 yield and selectivity (Figure 3.4a). Interestingly, power consumptions mirrored the coke formation profile, suggesting that coke deposition plays a significant role in affecting the power consumptions. From the results, lower power consumptions occurred with less coke formation were found at the input frequency of 300 Hz. It was selected as an optimum value for further investigation.

3.3.4. Effect of Electrode Gap Distance

For the investigation of the effect of electrode gap distance on the reforming reaction performance of the simulated natural gas, the electrode gap distance was varied in the range of 4-8 mm, while a steam content of 10 mol%, a HCs-to-O_2 feed molar ratio of 2/1, a total feed flow rate of 100 cm^3/min, an applied voltage of 14.5 kV, and input frequency of 300 Hz were used as the optimum conditions to operate the gliding arc system. The corresponding residence times at various electrode gap distances of 4, 6, 7, and 8 mm were 1.09, 1.37, 1.57, and 1.65 s, respectively. Beyond the highest electrode gap distance of 8 mm, the gliding arc system could not provide a steady discharge, whereas, at any electrode gap distance shorter than 4 mm, the system produced a large quantity of coke filaments across the two electrodes with in a relatively short operation period, causing a drastic drop of current and the termination of discharge.

The effects of the electrode gap distance on the reactant conversions and product yields are illustrated in Figure 3.5a. The conversions of CH_4, C_2H_6, C_3H_8, and O_2, as well as the H_2, CO, and C_2 yields, significantly increased with increasing electrode gap distance from 4 to 7 mm. The increase in the electrode gap distance simply increases the reaction volume and subsequently the residence time of gaseous species in the plasma zone increases. As a result, there is higher possibility of collisions between reactant molecules and electrons, leading to increases in all the reactant conversions (except CO_2) and product yields. These results are in good agreement with the significant decreases in the CH_4, C_2H_6, C_3H_8, and O_2 concentrations and the increases in the H_2 and CO concentrations in the outlet gas (Figure 3.5b). However, it was found that increasing the electrode gap distance in the range of 7-8 mm only slightly increased the CH_4, C_2H_6, C_3H_8, and O_2 conversions, as well as H_2, CO, and C_2 yields. It should be noted that there is another vital factor, apart from residence time, that affects the reactant conversions, product selectivities, and yields. When the electrode gap distance is varied, principally, the breakdown voltage required for initiating the plasma discharges and the power required for sustaining the discharges increase with increasing electrode gap distance [26]. However, if the electrode gap distance is too wide, the electric field strength weakens, resulting in a lower average electron energy, as well as a reduction in the number of electrons, which corresponds very well with the decreasing tendency of the generated current in the electrode gap distance range of 6 to 8 mm, as clearly shown in Figure 3.5c. Hence, all reactant conversions and product yields remained almost unchanged with increasing gap distance in this range, despite a longer residence time. Moreover, the results of the reactant conversions and product yields at different ranges of electrode gap

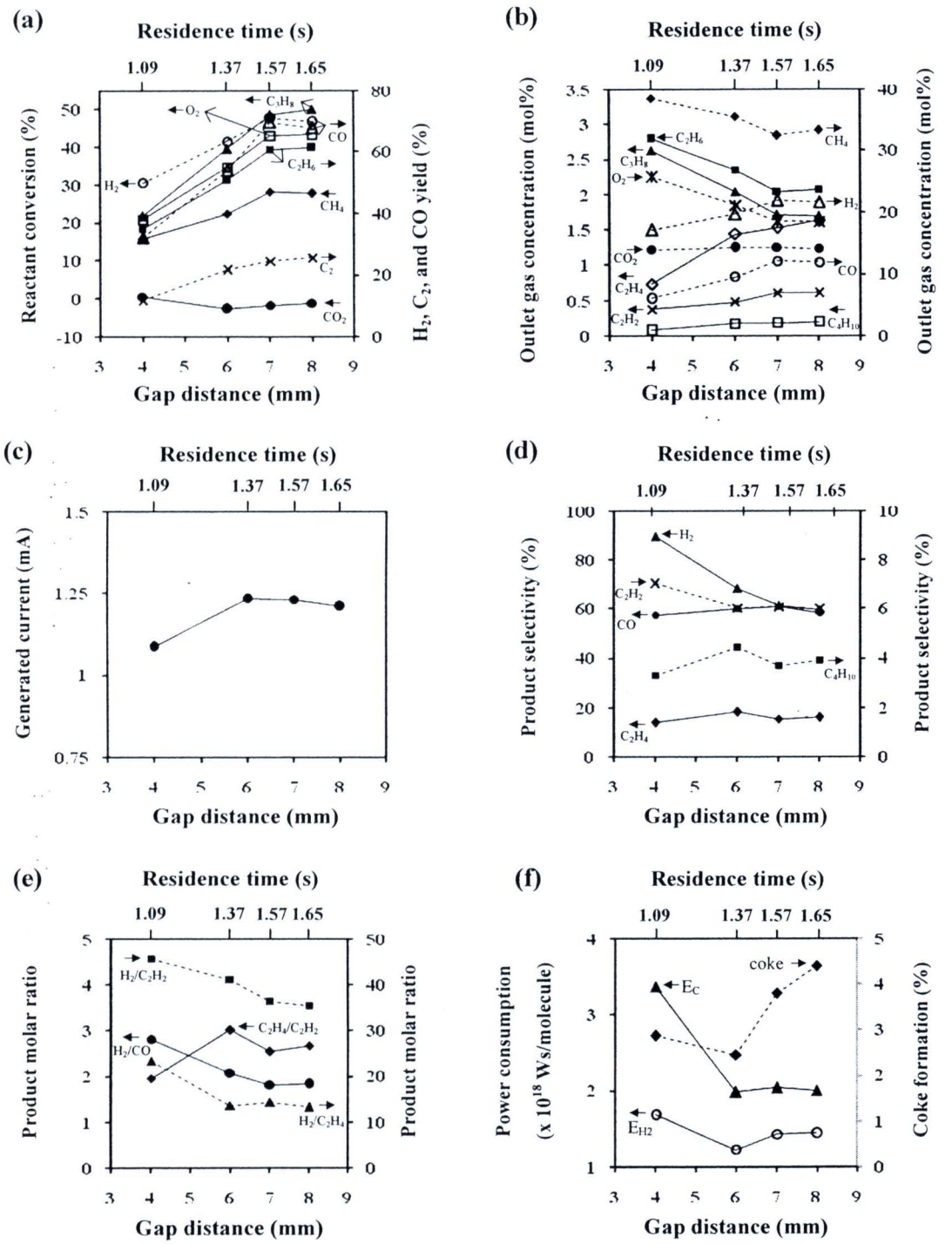

Figure 3.5 Effects of electrode gap distance on (a) reactant conversions and product yields, (b) concentrations of outlet gas, (c) generated current, (d) product selectivities, (e) product molar ratios, and (f) power consumptions and coke

formation under studied conditions: steam content, 10 mol%; HCs/O_2 feed molar ratio, 2/1; total feed flow rate, 100 cm^3/min; applied voltage, 14.5 kV; and input frequency, 300 Hz (E_c: power per reactant molecule converted; E_{H2}: power per H_2 molecule produced).

widths indicate that for the narrow electrode gap distance range of 4-6 mm, the residence time plays a dominant role in enhancing the plasma reforming performance, whereas, for the greater electrode gap distance range of 6-8 mm, the discharge characteristics have more significant impacts.

Figure 3.5d presents the effect of electrode gap distance on the product selectivities. The H_2 and C_2H_2 selectivities significantly decreased with increasing electrode gap distance. It may be implied that the increase in current by tapering electrode gap distance is responsible for the enhancement of the oxidative dehydrogenation reactions and the coupling reactions of the active species to form H_2 and C_2H_2. On the other hand, the C_2H_4 and C_4H_{10} selectivities tended to slightly increase with the expansion of electrode gap distance from 4 to 6 mm but beyond the electrode gap distance of 6 mm, they slightly decreased. These initial increases in both the C_2H_4 and C_4H_{10} selectivities suggest that the coupling reactions to obtain C_2H_4 and C_4H_{10} (Equations 44-47 and 53-54) more favorably occur than with the oxidative dehydrogenation reactions at a wider electrode gap distance (a longer residence time). A plausible explanation is that with wider electrode gap distance, the active species of hydrocarbons can further recombine via the coupling reactions due to the increase in residence time. However, when widening the electrode gap distance from 6 to 8 mm, all the product selectivities tended to slightly decrease probably due to both the decrease in

generated current, as described earlier, and the drastic increase in coke formation, as shown next. The CO selectivity varied slightly with a wider electrode gap distance, suggesting that the CO selectivity is independent of the electrode gap distance under the studied conditions.

Figure 3.5e illustrates the effect of the electrode gap distance on various product molar ratios. The molar ratios of H_2/CO, H_2/C_2H_2, and H_2/C_2H_4 greatly decreased with increasing electrode gap distance from 4 to 6 mm and then only slightly decreased with further widening of the electrode gap distance to 8 mm, whereas the C_2H_4/C_2H_2 molar ratio showed the opposite trend. These results again confirm that the coupling reactions of the active species more preferentially occur as secondary reactions than the dehydrogenation reactions when the system is operated at a longer residence time.

The power consumptions both per reactant molecule converted and per H_2 molecule produced decrease significantly with widening electrode gap distance from 4 to 6 mm and they tend to increase slightly with further widening of the electrode gap distance from 6 to 8 mm, as depicted in Figure 3.5f. The initial decrease in both power consumptions can be explained by the increases in the CH_4, C_2H_6, C_3H_8, and O_2 conversions, as well as the H_2 yield (Figure 3.5a). Beyond the electrode gap distance of 6 mm, which provided the minimum power consumptions, an increase in coke formation with further widening electrode gap distance is responsible for the increase in power consumptions.

3.3.5. Comparisons of CO_2-Containing Natural Gas Conversion Performances with Different Reforming Processes

Table 1 shows the comparisons of CO_2-containing natural gas conversion

performances, i.e. H_2 and CO selectivities and yields as well as power consumptions, with different reforming processes under their corresponding optimum conditions. It can be seen that the steam reforming process provided the highest H_2 selectivity of about 65.8%, but gave a very low CO selectivity of about 4.8%, as compared to the other reforming processes. Even though the highest H_2 selectivity was not obtained, the combined steam reforming and partial oxidation process gave acceptably high H_2 and CO selectivities of about 68.2% and 59.9%, respectively. As shown in Table 1, the significant enhancement of both the H_2 and CO selectivities for the combined steam reforming and partial oxidation process, as compared to all the other reforming processes. Both the steam and O_2 additions to the natural gas feed provides much higher number of oxygen active species, hydroxyl active species, and hydrogen active species (Equations 25-29). This enhances both the oxidative dehydrogenation reactions and coupling reactions (Equations 9-24, and 30-54). Interestingly, the combined steam reforming and partial oxidation process gives a very high CO production, as compared to the steam reforming process. This is because the added oxygen in the system can significantly suppress the coke formation, resulting in increased opportunities for CO formation (Equations 55-59). Hence, it can be clearly seen that the addition of both steam and oxygen can offer the acceptably highest synthesis gas production.

The power consumptions both per reactant molecule converted and per H_2 molecule produced are also given in Table 1. The results indicate that the presence of either oxygen (the combined reforming and partial oxidation process) or steam (the steam reforming process) in the natural gas feed could lower the power consumptions both per reactant molecule converted and per H_2 molecule produced, as compared to the case

Table 3.1 Comparison of the CO_2-containing natural gas conversion performances with different processes under their corresponding optimum conditions

Process	Operating conditions						Selectivity (%)		Yield (%)		Power consumptions ($\times 10^{18}$ s/molecule)	
	HCs/O_2 molar ratio	Steam content (mol%)	Total feed flow rate (cm^3/min)	Applied voltage (kV)	Input frequency (Hz)	Electrode gap distance (mm)	H_2	CO	H_2	CO	Per reactant molecule converted (E_C)	Per H_2 molecule produced (E_{H2})
Non-oxidative reforming[a]	-	-	125	15.5	300	6	24.5	2.9	12.2	-	6.34	3.58
Combined reforming and partial oxidation[b]	2/1	-	125	17.5	300	6	40.5	21.9	58.1	61.6	2.73	2.49
Steam reforming[c]	-	10	100	13.5	300	6	65.8	4.8	40.3	3.1	2.26	1.58
Combined steam reforming and partial oxidation[d]	2/1	10	100	14.5	300	6	68.2	59.9	63.4	54.0	1.98	1.22

[a][7], [b][10], [c][26], and [d]Present work

without the O_2 and steam addition (the sole reforming or non-oxidative reforming). The lowest power consumptions both per reactant molecule converted and per H_2 molecule produced were obtained from the combined steam reforming and partial oxidation process in the present work, suggesting that there is a synergistic effect of reduction in power consumption.

3.4 Conclusions

In this work, the combined steam reforming and partial oxidation of CO_2-containing natural gas was employed for the synthesis gas production from CO_2-containing natural gas in an AC gliding arc discharge system. The effects of the applied voltage, input frequency, and electrode gap distance significantly affected the reactant conversions, product selectivities, and product yields were investigated. The optimum conditions were found at a HCs/O_2 feed molar ratio of 2/1, an applied voltage of 14.5 kV, an input frequency of 300 Hz, and an electrode gap distance of 6 mm, which provided high CH_4 and O_2 conversions with high synthesis gas selectivity and very low power consumptions. Under these optimum conditions, the power consumptions were as low as 1.98×10^{-18} Ws (12.35 eV) per molecule of converted reactant and 1.22×10^{-18} Ws (7.64 eV) per molecule of produced hydrogen.

References

[1] SW. Yang, JN. Kondo, K. Hayashi, M. Hirono, K. Domen, H. Hosono. Partial oxidation of methane to syngas over promoted C12A7. Applied Catalysis A: General 227 (2004) 239-246.

[2] N.R. Bruke, DL. Trimm. Co-generation of energy and synthesis gas by partial oxidation of methane. Catalysis Today 117 (2006) 248-252.

[3] R.C. Vasant, C.M. Kartick. CO_2 reforming of methane combined with steam reforming or partial oxidation of methane to syngas over $NdCoO_3$ perovskite-type mixed metal-oxide catalyst. Applied Energy 83 (2006) 1024-1032.

[4] W. Yu, T. Ohmori, S. Kataoka, T. Yamamoto, A. Endo, M. Nakaiwa, N. Itoh. A comparative simulation study of methane steam reforming in a porous ceramic membrane reactor using nitrogen and steam as sweep gases. International Journal of Hydrogen Energy 33 (2008) 685-692.

[5] S. Ryi, J. Park, D. Kim, T. Kim, S. Kim. Methane steam reforming with a novel catalytic nickel membrane for effective hydrogen production. Journal of Membrane Science 339 (2009) 189-194.

[6] C.R.M. Santos, M. Laureanny, B.P. Fabio. The effect of the addition of Y_2O_3 to Ni/α-Al_2O_3 catalysts on the autothermal. Catalysis Today 149 (2010) 401-406.

[7] N. Rueangjitt, C. Akarawitoo, T. Sreethawong, S. Chavadej. Reforming of CO_2-containing natural gas using an AC gliding arc system: Effect of gas component in natural gas. Plasma Chemistry and Plasma Processing 27 (2007) 559-576.

[8] T. Sreethawong, P. Thakonpatthanakun, S. Chavadej. Partial oxidation of methane

with air for synthesis gas production in a multistage gliding arc discharge system. International Journal of Hydrogen Energy 32 (2007) 1067-1079.

[9] J.A. Anderson, M.F. Garcia. Supported Metals in Catalysis. Imperial College Press, 2005.

[10] N. Rueangjitt, T. Sreethawong, S. Chavadej. Reforming of CO_2-containing natural gas using an AC gliding arc system: effects of operational parameters and oxygen addition in feed. Plasma Chemistry and Plasma Processing 28 (2008) 49-67.

[11] B. Wang, X. Zhang, Y. Liu, G. Xu. Conversion of CH_4, steam and O_2 to syngas and hydrocarbons via dielectric barrier discharge. Journal of Natural Gas Chemistry 18 (2009) 94-97.

[12] M.G. Sobacchi, A.V. Saveliev, A.A. Fridman, L.A. Kennedy, S. Ahmed, T. Krause. Experimental assessment of combined plasma/catalytic system for hydrogen production via partial oxidation of hydrocarbon fuels. International Journal of Hydrogen Energy 27 (2002) 635-642.

[13] J.X. He, Y.Y. Han, A.H. Gao, Y.S. Zhou, Z.G. Lu. Investigation on methane decomposition and the formation of C_2 hydrocarbons in DC discharge plasma by emission spectroscopy. Chinese Journal of Chemical Engineering 12 (2004) 149-151.

[15] T. Nozaki, A. Hattori, K. Okazaki. Partial oxidation of methane using a microscale non-equilibrium plasma reactor. Catalysis Today 98 (2004) 607-616.

[15] C.S. Kalra, A.F. Gutsol, A.A. Fridman. Gliding arc discharge as a source of intermediate plasma for methane partial oxidation. IEEE Transactions on Plasma Science 33 (2005) 32-4.

[16] T. Paulmier, L. Fulcheri. Use of non-thermal plasma for hydrocarbons reforming.

Chemical Engineering Journal 106 (2005) 59-71.

[17] Y. Wang, C.J. Liu, Y.P. Zhang. Plasma methane conversion in the presence of dimethyl ether using dielectric-barrier discharge. Energy & Fuels 19 (2005) 877-881.

[18] E. El Ahmar, C. Met, O. Aubry, A. Khacef, J.M. Cormier. Hydrogen enrichment of a methane-air mixture by atmospheric pressure plasma for vehicle applications. Chemical Engineering Journal 116 (2006) 13-18.

[19] G. Petitpas, J.-D. Rollier, A. Darmon, J. Gonzalez-Aguilar, R. Matkemeijer, L. Fulcheri. A comparative study of non-thermal plasma assisted reforming technologies. International Journal of Hydrogen Energy 32 (2007) 2848-2867.

[20] Y.C. Yang, B.J. Lee, Y.N. Chun. Characteristics of methane reforming using gliding arc reactor. Energy 34 (2009) 172-177.

[21] C. Liu, A. Marafee, B. Hill, G. Xu, R. Mallinson, L. Lobban. Oxidative coupling of methane with ac and dc corona discharges. Industrial & Engineering Chemistry Research 35 (1996) 3295-3301.

[22] N. Rueangjitt, W. Jittiang, K. Pornmai, J. Chamnanmanoontham, T. Sreethawong, S. Chavadej. Combined reforming and partial oxidation of CO_2-containing natural gas using an AC multistage gliding arc system: effect of number of plasma reactors. Plasma Chemistry and Plasma Processing 29 (2009) 433-453.

[23] K. Pornmai, H. Sekiguchi, S. Chavadej. Synthesis gas production from reforming of CO_2-containing natural gas with steam using an AC gliding arc discharge system: effects of steam addition in feed and operational parameters. Plasma Sources Science and Technology (In Contribution).

[24] T. Zielinski, J. Kijenski. Plasma carbon black the new active additive for plastic.

Composites Part A : Applied Science and Manufacturing 36 (2005) 467-471.

[25] T. Opalinska, T. Zielinski, K. Schmidt-Szalowski. Carbon black generation in gliding arc discharges. Polish Journal of Chemistry 77 (2003) 1357-1361.

[26] K. Supat, A. Kruapong, S. Chavadej, L.L. Lobban, G.R. Millinson. Synthesis gas production from partial oxidation of methane with air in AC electric gas discharge. Energy & Fuels 17 (2003) 471-481.